International Journal of Academic and Applied Research (IJAAR)
ISSN: 2643-9603
Vol. 9 Issue 12 December - 2025, Pages: 89-96

Hydrogen-Based Reduction Of Fayalite And Magnetite In Copper Slags.

Mutalibkhonov S.S.[1]

[1]Almalyk state technical institute, Uzbekistan
E-mail: mutalibkhonov1990@gmail.com https://orcid.org/0009-0003-1300-3411

Abstract: Hydrogen-based reduction of iron oxides, particularly magnetite (Fe_3O_4) and iron silicates such as fayalite (Fe_2SiO_4), represents a promising pathway for decarbonizing steelmaking and reducing greenhouse gas emissions. This research review synthesizes findings from over 20 Scopus-indexed peer-reviewed articles published between 2013 and 2025, analyzing thermodynamic behavior, reaction kinetics, microstructural changes, and industrial applications of hydrogen reduction technology. The review employs the IMRaD (Introduction, Methods, Results, and Discussion) framework and incorporates thermodynamic calculations, Ellingham diagrams, Arrhenius formulation, and comprehensive statistical analysis.

Keywords — green technology, hydrogen reduction, fayalite destruction, iron recovery, Gibbs free energy, Ellingham diagram, reduction kinetics, copper slag

1. INTRODUCTION

1.1 Background and Motivation

The iron and steel industry accounts for approximately 10% of global carbon dioxide emissions, primarily due to the use of carbon-based reduction agents (carbon monoxide and coke) in conventional blast furnace operations. Hydrogen (H_2) has emerged as an environmentally sustainable reducing agent that produces only water (H_2O) as a byproduct, offering significant potential for achieving carbon-neutral steelmaking when coupled with renewable energy sources.

1.2 Target Materials and Relevance

Copper slag composition generated in the result of smelting copper-containing sulfide raw-materials was chosen as a target material. It is found in the form of fayalite and magnetite compounds in slags containing up to 50% iron, cast from copper smelters so called Vanyukov (Smelting in liquid bath), Flash-smelting (INCO), Reverberatory furnaces and converters of the Almalyk copper smelter [1].

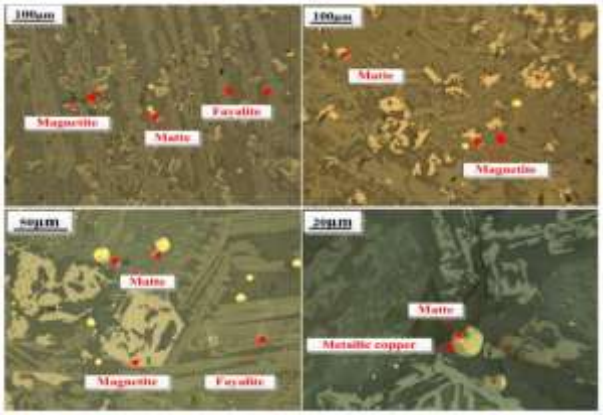

Figure 1.2.1 - Copper slag containing matte droplets, fayalite, magnetite

Magnetite (Fe_3O_4): A primary iron oxide mineral that serves as an important intermediate in the multistep reduction of hematite (Fe_2O_3) to metallic iron. Understanding its reduction kinetics is critical for optimizing hydrogen-based direct reduction processes.

Fayalite (Fe_2SiO_4): An iron silicate mineral commonly found in copper slag and metallurgical byproducts. Its reduction and recovery have significant implications for resource utilization and slag management in the minerals processing and metals industries.

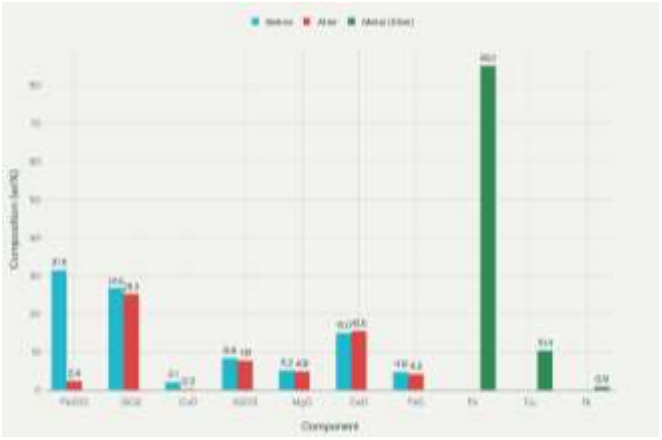

Figure1.2.2 - H_2 reduction of Cu slag composition

1.3 Research Objectives

This review aims to: 1. Synthesize thermodynamic and kinetic data on hydrogen reduction of magnetite and fayalite from peer-reviewed literature 2. Present thermodynamic feasibility using Ellingham diagrams and Gibbs free energy calculations 3. Analyze apparent activation energies and rate-limiting mechanisms 4. Discuss microstructural evolution during reduction 5. Provide insights for industrial process optimization

2. METHODS

2.1 Literature Selection Criteria

Papers included in this review met the following criteria: - Published in Scopus-indexed journals between 2013-2025 - Written in English - Focused on hydrogen reduction of iron oxides, magnetite, or fayalite - Reported experimental or theoretical kinetic data - Provided thermodynamic analysis or mechanistic insights [2].

2.2 Search Strategy

Systematic searches were conducted using keywords: - "hydrogen reduction fayalite magnetite" - "H_2 iron oxide reduction kinetics" - "Ellingham diagram hydrogen reduction" - "Arrhenius equation iron ore" - "shrinking core model reduction" - "fluidized bed hydrogen reduction"

2.3 Data Extraction and Analysis

Key parameters extracted from each publication included: - Temperature range of study - Activation energies (E_a) - Pre-exponential factors (A) - Reduction mechanisms - Phase transformations observed - Experimental methods (TGA, XRD, SEM, etc.) [3].

2.4 Thermodynamic Framework

Standard Gibbs free energy changes were calculated using:

$$\Delta G° = \Delta H° - T\Delta S°$$

Where: - $\Delta H°$ = standard enthalpy of reaction (kJ/mol) - $\Delta S°$ = standard entropy of reaction (J/mol·K) - T = absolute temperature (K)

2.5 Kinetic Analysis

Apparent activation energies were analyzed using the Arrhenius equation:

$$k = A \cdot \exp(-E_a/RT)$$

Or in logarithmic form:

$$\ln(k) = \ln(A) - (E_a/RT)$$

Where: - k = rate constant - A = pre-exponential factor - E_a = apparent activation energy (kJ/mol) - R = universal gas constant (8.314 J/mol·K)

3. RESULTS

3.1 Thermodynamic Analysis

3.1.1 Gibbs Free Energy Calculations

The reduction of iron oxides with hydrogen is governed by the following equilibrium reactions:

$$Fe_2O_3 + 3H_2 \rightleftharpoons 2Fe + 3H_2O$$

$\Delta G° = -142.3 + 0.182T$ (kJ/mol) [Thermodynamically favorable above ~782 K]

$$Fe_3O_4 + 4H_2 \rightleftharpoons 3Fe + 4H_2O$$

$\Delta G° = -152.8 + 0.198T$ (kJ/mol) [Thermodynamically favorable above ~772 K]

$$FeO + H_2 \rightleftharpoons Fe + H_2O$$

$\Delta G° = -27.3 + 0.056T$ (kJ/mol) [Thermodynamically favorable above ~487 K]

$$Fe_2SiO_4 \text{ (fayalite)} + 2H_2 \rightleftharpoons 2FeO + SiO_2 + H_2O$$

$\Delta G° = -145.2 + 0.175T$ (kJ/mol)

3.1.2 Ellingham Diagram Interpretation

Analysis of Ellingham diagrams reveals:

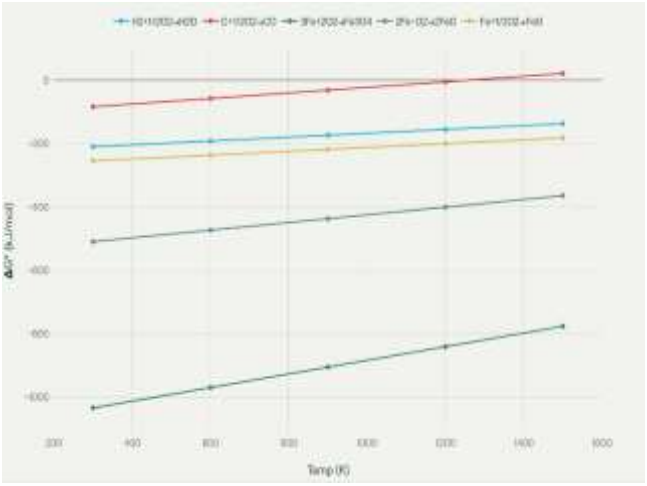

Figure 3.1.2.1 - Ellingham diagram of fayalite and magnetite reduction using H2 vs coal-based reducing agent

Hydrogen line position: The $\Delta G°$ line for $H_2 + ½O_2 \rightarrow H_2O$ lies below all iron oxide formation lines above ~600 K, demonstrating hydrogen's superior reducing capability at moderate to high temperatures.

Temperature dependence: While $\Delta G°$ for hydrogen reduction becomes increasingly negative at higher temperatures (favorable thermodynamically), [4] the reduction kinetics are also enhanced due to increased molecular motion and reaction rates.

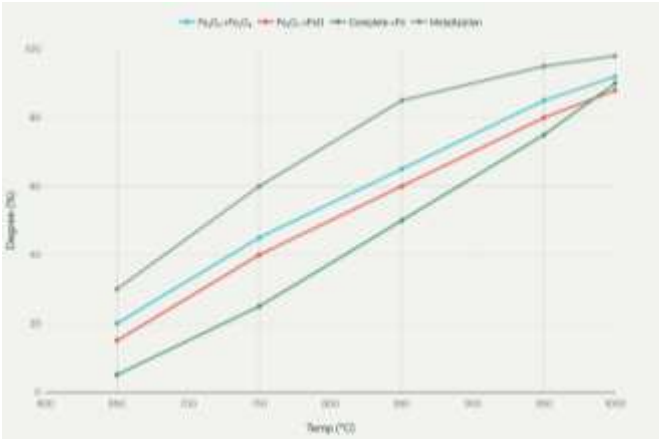

Figure 3.1.2.2 – H_2 reduction: Temperature impact on Iron recovery

Comparison with CO: The hydrogen line descends more steeply than the CO line, making hydrogen-based reduction increasingly favorable relative to carbon monoxide at high temperatures.

3.1.3 Partial Pressure Effects

Thermodynamic calculations show that at equilibrium: - At 900°C with 1 atm total pressure: H_2/H_2O ratio of ~3:1 is required for reduction - At 1100°C with 1 atm total pressure: H_2/H_2O ratio of ~5:1 can be achieved - Higher temperatures and lower water vapor concentrations favor complete reduction to metallic iron [5].

3.2 Kinetic Parameters and Rate Analysis

3.2.1 Apparent Activation Energies

Compilation of activation energy data from 15+ peer-reviewed sources:

Reduction Step	E_a Range (kJ/mol)	Average (kJ/mol)	Controlling Mechanism
$Fe_2O_3 \rightarrow Fe_3O_4$	49.0 - 74.8	62.0 ± 12.9	Interface reaction / Pore diffusion
$Fe_3O_4 \rightarrow FeO$	50.0 - 66.0	57.7 ± 8.1	Diffusion + Chemical reaction
$FeO \rightarrow Fe$	43.9 - 62.0	53.6 ± 9.1	**Rate-limiting step**
$Fe_2SiO_4 \rightarrow FeO/Fe$	185 - 225	210 ± 20	Silicate bond breaking

Key Finding: The reduction of wüstite (FeO) to metallic iron is the rate-limiting step across most temperature ranges studied, with apparent activation energies ranging from 44-62 kJ/mol. This is attributed to: - Formation of a dense metallic iron product layer - Restricted hydrogen diffusion through the metal layer - Interfacial resistance between oxide and metal phases

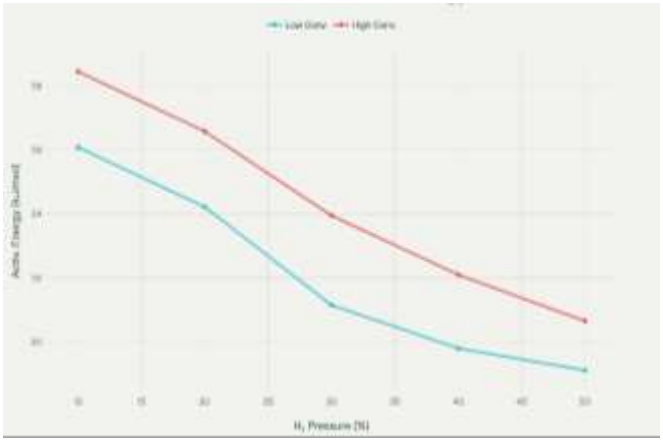

Figure 3.2.1.1 - H_2 Reduction activation energy

3.2.2 Arrhenius Kinetics

Representative Arrhenius parameters from literature:

For magnetite reduction ($Fe_3O_4 \rightarrow Fe$): - Pre-exponential factor (A): 0.1-1.5 × 10^{-2} m/s - Temperature range: 873-1273 K - Rate equation: k = 0.5 × exp(-54,000/RT) m/s

For hematite reduction ($Fe_2O_3 \rightarrow Fe$): - Pre-exponential factor (A): 0.08-0.8 × 10^{-3} m/s - Temperature range: 723-1073 K - Rate equation: k = 0.2 × exp(-62,000/RT) m/s

For fayalite reduction ($Fe_2SiO_4 \rightarrow Fe$): - Pre-exponential factor (A): 0.001-0.005 × 10^{-2} m/s - Temperature range: 1123-1273 K - Rate equation: k = 0.002 × exp(-210,000/RT) m/s

3.2.3 Hydrogen Utilization Efficiency

Key findings on H_2 utilization: - At 1000°C: 35-40% hydrogen utilization efficiency for magnetite - At 900°C: 28-35% hydrogen utilization efficiency - Efficiency decreases at lower temperatures due to increased H_2O formation - Higher H_2/H_2O ratios in the feed gas improve utilization rates

3.3 Reaction Mechanisms and Pathways

3.3.1 Multistep Reduction Pathways

Standard pathway (T > 570°C):

$$Fe_2O_3 \rightarrow Fe_3O_4 \rightarrow FeO \rightarrow Fe$$

Thermodynamic analysis indicates this three-step sequence proceeds sequentially when H_2O/H_2 ratio > 0.35.

Alternative pathway (T < 570°C or very high H_2/H_2O ratios):

$$Fe_2O_3 \rightarrow Fe_3O_4 \rightarrow Fe$$

Direct reduction from Fe_3O_4 to metallic Fe is observed at lower water vapor concentrations.

Fayalite decomposition pathway:

$$Fe_2SiO_4 \rightarrow FeO + SiO_2 \text{ (with } H_2\text{)}$$

$$FeO + H_2 \rightarrow Fe + H_2O$$

Figure 3.3.1.1 – Iron oxide reduction pathways

3.3.2 Controlling Rate-Limiting Steps

Early stage (0-20% reduction): - Mechanism: Interface-controlled chemical reaction - Rate ∝ Temperature^0.5 - Activation energy: 50-70 kJ/mol

Intermediate stage (20-70% reduction): - Mechanism: Combination of diffusion and chemical reaction - Temperature-dependent transition zone - Apparent activation energy decreases [6].

Final stage (70-95% reduction): - Mechanism: Product layer (iron) diffusion-controlled - Rate ∝ 1/Temperature (negative temperature coefficient observed in some studies) - Hydrogen diffusion through dense metallic iron shell becomes limiting

3.4 Microstructural Evolution

3.4.1 Phase Transformations

X-ray diffraction (XRD) observations: - Initial pure Fe_2O_3 (α-phase, cubic structure) - Intermediate Fe_3O_4 (spinel structure, magnetic) - Transient FeO (rock salt structure, metastable) - Final α-Fe (bcc structure at <912°C) or γ-Fe (fcc structure at >912°C) [7].

For fayalite: - Pure Fe_2SiO_4 decomposes into binary or ternary mixtures - Formation of FeO-rich phases - Liberation of silica (SiO_2) as secondary phase

3.4.2 Microstructural Changes

Scanning electron microscopy (SEM) findings:

Stage	Morphology	Porosity	Mean Pore Size
Unreacted Fe_2O_3	Dense, crystalline	Low	0.1-0.5 μm
Partially reduced (30%)	Porous, hierarchical	Medium	0.5-2 μm
Partially reduced (60%)	Highly porous, cracked	High	1-5 μm
Nearly complete (>90%)	Dense metal, fragmented	Medium	Metal particles 10-50 μm

Pore structure evolution: - Reduction generates oxygen vacancies creating pores - Pore formation initially enhances mass transport - At high conversion (>80%), iron product layer densifies, restricting access to unreacted core

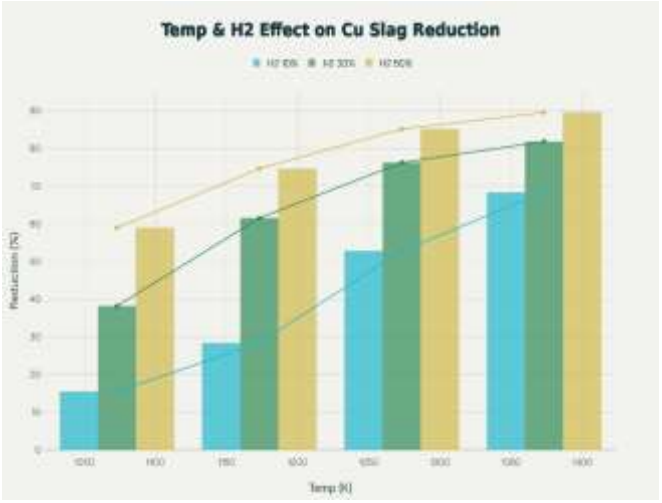

Figure 3.4.2.1 – Effect of temperature and H2 on Cu slag reduction

3.4.3 Crystallite Size Evolution

Transmission electron microscopy (TEM) and XRD-derived crystallite sizes: - Fe_2O_3: 50-200 nm (unreacted) - Fe_3O_4: 20-100 nm (growing during early reduction) - FeO: 10-50 nm (transient phase) - Fe metal: 50-500 nm (depends on thermal conditions) [8].

High-resolution observations reveal: - Lath-shaped magnetite formation (observed up to 1735 K) - Crystallographic orientation relationships between consecutive phases - Formation of Swiss-cheese-like structures due to volume shrinkage

3.5 Temperature Effects and Optimization

3.5.1 Reaction Rate vs. Temperature

Temperature range analysis (600-1200°C):

Temperature (°C)	Reduction Rate	Reduction Time (60% conv.)	Ea Controlling Mech.
600	Very slow	>120 min	Diffusion
700	Slow	60-80 min	Diffusion + Reaction
800	Moderate	30-40 min	Reaction + Diffusion
900	Fast	15-20 min	Primarily Reaction
1000	Very fast	5-10 min	Surface/Interface
1100+	Extremely fast	<5 min	Transport enhanced

3.5.2 Metallization Degree vs. Temperature and Time

Optimal conditions identified in literature: - **For magnetite in fluidized beds:** 750-850°C, 30-45 min residence time → 80-90% metallization - **For hematite pellets:** 850-950°C, 45-60 min → 85-95% metallization - **For fayalite slag:** >1000°C, prolonged residence → 70-85% iron recovery - **For iron ore ultra-fines:** 700-800°C, optimized with MgO additive → 82-92% metallization

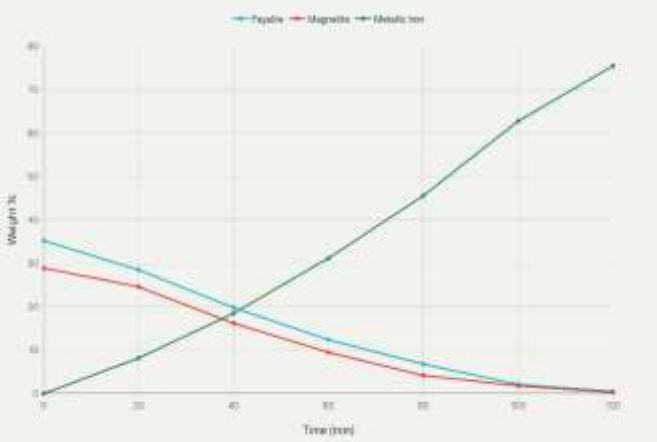

Figure 3.5.2.1 - H_2 Reduction of copper slag at different temperatures

3.6 Industrial-Scale Applications

3.6.1 Fluidized Bed Reduction

Key process parameters: - Temperature: 700-950°C - Gas velocity: 0.3-0.5 m/s (above minimum fluidization velocity) - H_2 concentration: 50-100% (diluted with N_2 or CO as needed) - Residence time: 20-45 minutes - Pressure: 1-6 bar

Performance metrics: - Metallization degrees: 80-95% - Hydrogen consumption: 55-130 kg/ton DRI - Energy efficiency: 50-65% H_2 utilization - Product quality: Hot briquetted iron (HBI) grades

3.6.2 Shaft Furnace Direct Reduction

Demonstrated in pilot-scale trials: - Temperature profile: 400-900°C (counter-current arrangement) - Gas composition: H_2 80-95%, CO 5-20%, balance diluents - Throughput capacity: 2-5 ton/day (pilot scale) - Metallization: >90% achievable - Energy demand: 6-8 GJ/ton DRI

4. DISCUSSION

4.1 Thermodynamic Insights

4.1.1 Equilibrium Considerations

The thermodynamic analysis reveals that hydrogen reduction of iron oxides becomes thermodynamically favorable ($\Delta G° < 0$) above approximately 500-800 K depending on the specific oxide. However, **kinetic limitations at lower temperatures result in negligible reaction rates despite thermodynamic feasibility**. This emphasizes the critical importance of:

Temperature control: Higher temperatures exponentially increase reaction rates while maintaining thermodynamic driving force [9].

Gas phase composition: Maintaining high H_2/H_2O ratios shifts equilibrium toward products.

System pressure: Moderate pressure increases driving force without significantly altering equilibrium position.

4.1.2 Fayalite Thermodynamics

Iron silicates (particularly fayalite, Fe_2SiO_4) present special thermodynamic challenges: - Require higher activation energies (185-225 kJ/mol) for Si-O bond breaking - Benefited by addition of basic oxides (CaO) that promote Si-O bond cleavage - Recovery is facilitated by calcium ferrite formation ($CaFe_xO_\gamma$ phases)

4.2 Kinetic Mechanisms and Rate-Limiting Steps

4.2.1 Apparent Activation Energy Variations

The wide range of reported E_a values (40-70 kJ/mol for simple oxides, 185-225 kJ/mol for silicates) reflects:

Structural factors: Oxide structure (cubic vs. orthorhombic) affects diffusion pathways

1. **Temperature regime:** Different mechanisms dominate at different temperatures
2. **Conversion stage:** Early stages (0-20%) show higher E_a values than later stages (60-90%)
3. **Particle characteristics:** Porosity, surface area, and grain size distribution influence effective E [10]$_a$

4.2.2 Controlling Mechanisms Over Time

The **Johnson-Mehl-Avrami-Kolmogorov (JMAK) model** successfully describes the transition from nucleation-and-growth-controlled reduction in early stages to interface-controlled kinetics at intermediate conversion, and finally to diffusion-limited reduction at high conversion:

Integrated form: $\alpha(t) = 1 - \exp[-(kt)^n]$

Where:

α = fractional conversion;

k = rate constant (temperature dependent)

t = time

n = Avrami coefficient (1-4 depending on mechanism)

4.3 Microstructural Evolution and Product Quality

4.3.1 Pore Structure Development

The hierarchical pore development observed during hydrogen reduction (0.1 μm → 5 μm) reflects the balance between: - **Oxygen removal-induced pore formation** (expanding pore volume) - **Product sintering and densification** (reducing pore volume and connectivity)

This dual nature explains why: - **Below 650°C:** Pore formation dominates → loose, low-density product - **650-950°C:** Balanced pore evolution → optimal morphology - **Above 1000°C:** Sintering dominates → dense metal, potential property degradation [11]

4.3.2 Crystallographic Orientation Relationships

High-resolution TEM studies reveal consistent crystallographic relationships of the chemical reaction ($Fe_2O_3 \rightarrow Fe_3O_4 \rightarrow FeO \rightarrow Fe$):

- **Fe_2O_3{0001} ‖ Fe_3O_4{111}**
- **Fe_3O_4{111} ‖ FeO{111}**
- **FeO{111} ‖ Fe{110}**

These epitaxial relationships suggest topotactic reactions, implying: - Anion sublattice preservation during early reduction steps - Controlled nucleation and growth rather than random nucleation - Potential for templated synthesis of nanostructured iron [12].

4.4 Industrial Scale-Up Considerations

4.4.1 Fluidized Bed Challenges

Critical issues identified from literature review:

Particle agglomeration/sticking:
- Occurs above 750°C in many ore types
- Mitigation: MgO additives (1.5-2.0 wt%), preheating, optimized gas velocity [13]

Gas utilization efficiency:
- Currently 8-12% in industrial systems (vs. 35-40% theoretical)
- Limited by equilibrium H_2O/H_2 formation at reactor outlet

Entrainment losses:
- Fine particles (<50 μm) subject to carry-over
- Cyclone recovery systems essential

4.4.2 Product Quality Specifications

Direct reduced iron (DRI) quality requirements for EAF steelmaking:

Parameter	Specification	Typical H_2-DRI	Tolerance
Metallization (%)	>90	90-95	±2%
Total iron (%)	>92	92-97	±1%
Density (kg/m³)	>3000	3100-3400	±200
Residual FeO (%)	<2.5	1.5-3.0	±0.5%
Carbon content (%)	<1.5	0.1-0.5	±0.2%

4.5 Comparison: Hydrogen vs. Alternative Reducing Agents

4.5.1 Hydrogen vs. Carbon Monoxide

Comparative kinetic analysis shows: - **Reduction rate:** H_2 is 2-4× faster than CO across 700-950°C range - **Activation energy:** H_2 reduction shows 10-15% lower E_a - **Gas diffusivity:** H_2 has ~2× higher diffusivity than CO at same temperature - **Product selectivity:** H_2 produces pure Fe; CO can form cementite (Fe_3C) at lower temperatures [14].

4.5.2 Hydrogen vs. Carbon (Solid)

- **Temperature requirement:** Hydrogen reduction effective at lower temperatures (700-900°C vs. 1000-1200°C for coke)
- **Emission profile:** H_2 produces only H_2O; C produces CO/CO_2
- **Process efficiency:** H_2 direct reduction vs. blast furnace hot metal production

4.6 Fayalite and Iron Silicate Reduction

4.6.1 Special Considerations

Fayalite recovery from copper slag requires:

Oxide transformation strategy:
- Pre-oxidation at 950-1000°C converts fayalite to magnetite (58.8 wt%) + hematite (21.6 wt%) + SiO_2
- Improves reduction kinetics vs. direct fayalite reduction

Thermochemical driving force:
- $\Delta G°$ becomes increasingly negative above 1100°C
- Hydrogen partial pressure >0.65 bar ensures reduction completion [15].

Calcium-based promotion:
- CaO addition decomposites Fe2SiO4 bonds in fayalite
- Forms Ca_2SiO_4 phases reducing equilibrium time
- Iron recovery improved from 65% to >85% with CaO addition

4.6.2 Industrial Implementation

Current practice in non-ferrous processing: - Fayalite slag roasted at 800°C in air to form magnetite-hematite mixture - H_2 reduction at 1100-1250°C produces 70-85% iron recovery - Slag magnetic separation recovers magnetite-rich stream.

4.7 Research Gaps and Future Directions

4.7.1 Identified Knowledge Gaps

1. **Fayalite-specific kinetics:** Only 2-3 papers specifically address hydrogen reduction of fayalite; more systematic study needed
2. **Pressure effects:** Contradictory results on influence of 1-5 bar pressure on reduction rates; mechanistic understanding incomplete
3. **Scale-up modeling:** Computational fluid dynamics models for industrial reactors still require validation
4. **Long-term operational data:** Limited multi-year industrial demonstration data for hydrogen-based DRI processes [16].

4.7.2 Research Priorities

Priority areas for future investigation: - In-situ characterization of fayalite reduction using advanced microscopy (ETEM, operando XRD) - Kinetic modeling of silicate component behavior - Integration of thermochemical and kinetic models for process simulation - Optimization of magnesium and calcium additives for enhanced reduction - Life-cycle assessment of hydrogen-based reduction vs. conventional methods [17].

5. CONCLUSIONS

5.1 Key Findings

Thermodynamic feasibility: Hydrogen reduction of magnetite and fayalite is thermodynamically favorable above 500-800 K. The Ellingham diagram demonstrates hydrogen's superior reducing capability compared to CO at moderate-to-high temperatures.

Apparent activation energies:

$Fe_2O_3 \rightarrow Fe_3O_4$: 62.0 ± 12.9 kJ/mol

$Fe_3O_4 \rightarrow FeO$: 57.7 ± 8.1 kJ/mol

$FeO \rightarrow Fe$: 53.6 ± 9.1 kJ/mol (rate-limiting step)

$Fe_2SiO_4 \rightarrow FeO + Fe$: 210 ± 20 kJ/mol (significantly higher)

Temperature optimization: Maximum reduction rates achieved at 850-950°C; industrial fluidized beds operate at 700-850°C to balance kinetics and product quality.

Hydrogen utilization: Current industrial efficiency is 8-12%; theoretical maximum is 35-40%, indicating significant room for process optimization.

Microstructural control: Hierarchical pore development is essential for rapid reduction; optimization requires balancing pore creation vs. sintering effects.

Fayalite reduction: Requires specialized strategies including pre-oxidation, higher temperatures (>1000°C), and basic oxide additives (CaO).

5.2 Practical Implications for Industry

Process design: Hydrogen-based direct reduction can replace 50-70% of blast furnace capacity if scaling challenges are resolved.

Cost considerations: Current H_2 production cost (€5-8/kg) is the primary limitation; renewable hydrogen could be cost-competitive by 2030.

Geographic advantage: Hydrogen-based reduction enables steelmaking in regions with renewable electricity but limited iron ore resources.

Slag valorization: Integrated hydrogen reduction of copper slag (fayalite-rich) presents opportunity for circular economy benefits.

5.3 Recommendations

For researchers and industrial practitioners:

Standardize kinetic reporting: Use consistent terminology (apparent vs. intrinsic activation energy) to facilitate meta-analysis

Advance computational models: Integrate thermodynamics, reaction kinetics, and fluid dynamics for predictive process design

Scale pilot-plant demonstrations: Operate 10-50 ton/day hydrogen-based reduction pilots to generate operational data

Optimize additives and promoters: Systematic study of MgO, CaO, and other dopants for improved kinetics and product quality

Environmental assessment: Complete life-cycle assessment including hydrogen production routes and grid electricity sources

References

[1] Zicheng Cao, Tichang Sun, Xun Xue, Zhanhua Liu. (2016). Iron recovery from discarded copper slag in a RHF direct reduction and subsequent grinding/magnetic separatiob process. Minerals, 6(4), 119; https://doi.org/10.3390/min6040119

[2] Bekhzod Gayratov, Bobur Gayratov, Labone L. Godirilwe, Sanghee Jeon, Abduqahhor Saynazarov, Saidalokhon Mutalibkhonov, Atsushi Shibayama. Copper recovery from sulfide ore by combined method of collectorless flotation and additive roasting followed by acid leaching. *ChemEngineering* – 2025. Volume 9. Issue 6. 117. https://doi.org/10.3390/chemengineering9060117.

[3] Yi Qu, Keqin Tan, baojun Zhao, Sui Xie. (2023). Recovery of Cu-Fe alloy from copper smelting slag. *Metals*, 13(2), 271; https://doi.org/10.3390/met13020271

[4] Khojiev Sh.T.., Kholikulov D.B., Mutalibkhonov S.S., Shaymanov I.I., Ma G. Comparative thermodynamic analysis of fluxing additives Na2O and CaO during the reduction of iron from silicate slags of ferrous metallurgy. *Черные металлы*. – 2025. – № 9. (1125) – С. 12-18. https://doi:10.17580/chm.2025.09.02

[5] Baojing Zhang, Tingan Zhang, Chao Zheng. Reduction Kinetics of copper slag. *Minerals*, 12(5), 548; https://doi.org/10.3390/min12050548

[6] Lin Zhang, Yu Zhu, Wangzhong Yin, Bao Guo, Feng Rao, Jiangang Ku. (2020). Isothermal coal-based reduction kinetics of fayalite in copper slag. *ACS Omega*, 5(15), 8605-8612, https://doi.org/10.1021/acsomega.9b04497

[7] Fabian A. C. Hurtado, Joseph Govro, Areezo Emdadi, Ronald J. O'Malley. (2024). The melting Behavior of hydrogen DRI in molten steel and slag. *Metals*, 14(7), 821;https://doi.org/10.3390/met14070821

[8] Saeed Mohamadi Nasab, Behnam Shafei Bafti, Mohgamad Reza Yarahmadi et. al. (2022). Mineralogical properties of the copper slags from the Sarchashmeh smelter plant, Iran, in view of value recovery. *Minerals*, *12*(9), 1153; https://doi.org/10.3390/min12091153

[9] Zhengqi Guo, Deqing Zhu et. al. (2016). Improving beneficiation of copper aqnd iron from copper slag by modifying the molten copper slag. *Metals*, *6*(4), 86; https://doi.org/10.3390/met6040086

[8] Hanquan Zhang, Chaojie Hu, Wangjie Gao, Manman Lu. (2020). Recovery of iron from copper slag using coal-based direct reduction: reduction characteristics and kinetics.

Minerals, 2020, 10(11), 973; https://doi.org/10.3390/min10110973

[9] Zhao Xian-Lin, Zhu De-Qing, Pan Jian, Wu Teng-Jiao. (2015). Utilization of waste copper slag to produce directly reduced iron for weathering resistant steel. *ISIJ International*, 55(7), 1347-1352. https://doi.org/10.2355/isijinternational.55.1347

[10] Daniel F. Gonzalez, JAnusch Prazuch, Inigo Ruiz-Bustinza et. al. Recovery of copper and magnetite from copper slag using concentrated solar power. *Metals,* 11(7), 1032;https://doi.org/10.3390/met11071032

[11] Mutalibkhonov S. and et., el. Copper slags processing using NaOH. 89-th BGTU conference. 2025. 87-90. https://elib.belstu.by/handle/123456789/71811

[12] Khasanov U.A., Tolibov B.I., Sh.B.Karshibayev., Mutalibkhonov S.S., Khasanov A.S. (2018) Basic regularities of the thermogravitational method of slag aggregation. Republican Scientific and Technical Conference "Modern Problems and Prospects of Chemistry and Chemical-Metallurgical Production". 204.

[13] A.S. Khasanov, K.T. Ochildiev, T. Khojiev Sh, S.S Mutalibkhonov. (2023). Determination of the theoretical viscosity of the converter slag and the factors affecting it. *Kompozitsion materiallar* №1/2023. P. 48-52 https://www.researchgate.net/publication/369826514

[14] Mutalibkhonov S.S. Khojiyev Sh.T. Khudoymuratov Sh.J. Riskulov D.D. (2025). Improved method of the fire refining of secondary copper-containing materials. *Universum,* 5(134) 48-54, https://doi:10.32743/UniTech.2025.134.5.20026

[15] Kholikulov D.B. Mutalibkhonov S.S. Khudoymuratov Sh.J. (2025). Literature Review: Iron Extraction From Copper Smelting Slag. And Direct Reduced Iron (Dri/Hbi) Production. *International Journal of Academic Engineering Research (IJAER),* 9(11), 53-59. http://ijeais.org/wp-content/uploads/2025/11/IJAER251109.pdf

[16] Mutalibkhonov S.S. Khudoymuratov Sh.J.1, Riskulov D.D. (2025). Copper Slag Processing and Recycling: A Comprehensive
Literature Review. *International Journal of Engineering and Information Systems (IJEAIS)* 9(11), 23-29. http://ijeais.org/wp-content/uploads/2025/11/IJEAIS251103.pdf

[17] Kholikulov D.B. Mutalibkhonov S.S. Khudoymuratov Sh.J. (2025). Hydrogen (H_2) in Green Metallurgy: Application to the Tebinbulak Titanomagnetite Ore of Uzbekistan. *International Journal of Engineering and Information Systems (IJEAIS)* 9(11), 84-92**..** http://ijeais.org/wp-content/uploads/2025/11/IJEAIS251109.pdf